

A PHYSICAL MODEL OF LYMAN ALPHA EMITTERS

VITHAL TILVI¹, SANGEETA MALHOTRA¹, JAMES E. RHOADS¹, EVAN SCANNAPIECO¹, ROBERT J. THACKER², ILIAN T. ILIEV^{3,4}, AND GARRELT MELLEMA⁵

ABSTRACT

We present a simple physical model for populating dark matter (DM) halos with Lyman Alpha Emitters (LAEs) and predict the physical properties of LAEs at $z \approx 3 - 7$. The central tenet of this model is that the Ly α luminosity is proportional to the star formation rate (SFR) which is directly related to the halo mass accretion rate. The only free parameter in our model is then the star-formation efficiency (SFE). An efficiency of 2.5% provides the best-fit to the Ly α luminosity function (LF) at redshift $z = 3.1$, and we use this SFE to construct Ly α LFs at other redshifts. Our model reproduce the Ly α LFs, stellar ages, $\text{SFR} \approx 1 - 10 M_{\odot} \text{ yr}^{-1}$, stellar masses $\sim 10^7 - 10^8 M_{\odot}$ and the clustering properties of LAEs at $z \approx 3 - 7$. We find the spatial correlation lengths $r_o \approx 3 - 6 h^{-1} \text{ Mpc}$, in agreement with the observations. Finally, we estimate the field-to-field variation $\approx 30\%$ for current volume and flux limited surveys, again consistent with observations. Our results suggest that the star formation, and hence Ly α emission in LAEs is powered by the accretion of new material, and that the physical properties of LAEs do not evolve significantly over a wide range of redshifts. Relating the accreted mass, rather than the total mass, to the Ly α luminosity of LAEs naturally gives rise to the duty cycle of LAEs.

Subject headings: galaxies: high-redshift — galaxies: Lyman alpha emitters — galaxy: luminosity function — galaxy: clustering — galaxy: correlation length

1. INTRODUCTION

Lyman- α emitting galaxies (LAEs), which seem to be powered by star formation activity, are selected on the basis of strong Ly α emission line, irrespective of other galaxy properties (e.g. Cowie & Hu 1998; Rhoads et al. 2000, 2004; Fynbo et al. 2001; Ajiki et al. 2003; Matsuda et al. 2005; Taniguchi et al. 2005; Gawiser et al. 2006; Shimasaku et al. 2006; Tapken et al. 2006; Murayama et al. 2007; Nilsson et al. 2007; Ouchi et al. 2008). However, the high-redshift galaxies selected on the basis of this one property are reasonably uniform in some of their other properties⁶. For example, the inferred stellar masses of LAEs at $z < 5$ are typically small, $\sim 10^6 - 10^9 M_{\odot}$ (Gawiser et al. 2006; Pirzkal et al. 2007; Finkelstein et al. 2007; Pentericci et al. 2009), and often have large Ly α equivalent width indicating a young stellar population (Malhotra & Rhoads 2002), which is also supported by the blue color of these galaxies (Venemans et al. 2005; Finkelstein et al. 2007, 2008; Gronwall et al. 2007; Pirzkal et al. 2007), especially at high redshifts. AGNs are ruled out as sources of strong Ly α emission in LAEs due to non-detection of X-ray emission (Malhotra et al. 2003; Wang et al. 2004; Gawiser et al. 2007) and lack of

high ionization lines in the optical spectra (Dawson et al. 2004, 2007). LAEs have a moderate SFR $\approx 5-8 M_{\odot} \text{ yr}^{-1}$ (e.g. Pirzkal et al. 2007; Taniguchi et al. 2005) and spatial correlation lengths of $\approx 3-5 h^{-1} \text{ Mpc}$, albeit with a substantial uncertainty (Ouchi et al. 2003; Kovač et al. 2007; Gawiser et al. 2007).

Despite the increasing number of LAE observations, theoretical understanding of LAEs is still in early stages primarily due to poor understanding of physical properties including star formation rate (SFR), stellar initial mass function, Ly α escape fraction, and the duty cycle of Ly α phase of star-forming galaxies at high redshifts. There have been several theoretical studies of LAEs based on cosmological simulations (e.g. Barton et al. 2004; Davé et al. 2006; Tasitsiomi 2006; Shimizu et al. 2007; Nagamine et al. 2008), semi-analytical models (e.g. Le Delliou et al. 2006; Kobayashi et al. 2007) and analytical models (e.g. Haiman & Spaans 1999; Dijkstra et al. 2007; Mao et al. 2007; Stark et al. 2007; Fernandez & Komatsu 2008) that relate the total halo mass to the Ly α luminosity of LAEs. Such a linear relationship between the halo mass and the Ly α luminosity often leads to an overprediction of the number density of LAEs. To reconcile the mass distribution of halos to the LF one needs to either assume a small escape fraction of Ly α photons (which would fail to account for the large Ly α EWs observed) or introduce a duty cycle (e.g. Stark et al. 2007; Nagamine et al. 2008) which adds another parameter to the models. In addition, the complexity and large number of variable parameters in many models motivates the development of a simple model that can reproduce the LAE observations over a wide range of redshifts. Such a model would be particularly useful in understanding the nature of LAEs observed at high redshifts.

In this paper we present a physical model to populate

¹ School of Earth and Space Exploration, Arizona State University, Tempe, AZ 85287 ; tilvi@asu.edu

² Saint Mary's University, Halifax, NS, Canada, B3H 3C3.

³ Universitaet Zuerich, Institut fuer Theoretische Physik, CH-8057 Zuerich, Switzerland.

⁴ Astronomy Centre, Department of Physics & Astronomy, Pevensy II Building, University of Sussex, Falmer, Brighton BN1 9QH, United Kingdom.

⁵ Dept. of Astronomy and Oskar Klein Centre, AlbaNova, Stockholm University, SE-10691 Stockholm, Sweden

⁶ In this paper we restrict our studies to only compact LAEs (at $z = 3 - 6.6$) detected using narrow-band excess. Other Ly α emitting objects (e.g. Ly α blobs and AGNs) are typically much more energetic and are probably fueled by AGN activity.

DM halos with LAEs in a cosmological simulation, and predict the abundances & physical properties of LAEs at $z \approx 3 - 7$. This model differs from many of the earlier studies in a major way, namely in that we relate mass accreted, as opposed to the total halo mass, to the Ly α luminosity. Mass accretion onto halos via smooth infall and accretion due to mergers of a specific mass ratios has been shown to have distinctly different clustering behaviour (Scannapieco & Thacker 2003). However, in this model we do not distinguish between the smooth accretion and the accretion due to mergers. In other words, in our model the LAEs are undergoing an episode of star-formation which is driven by accretion of fresh material onto the halos, independent of whether the accretion is due to mergers or if it is via smooth infall. While there is no direct observational evidence showing a relation between the baryons accreted and the Ly α luminosity, recent studies (e.g. Dekel et al. 2009; Kereš et al. 2009) have shown that such cold accretion of new material can drive star formation in galaxies, especially those hosted by less massive halos. In this model we assume that the LAEs do not contain large amounts of dust, and hence most of the hydrogen ionizing photons will be absorbed, while most of the Ly α photons can escape (Gawiser et al. 2006; Kobayashi et al. 2007). This assumption yields large Ly α equivalent widths even without appealing to metal-free Population III stars, whose contributions are constrained by non-detection of the HeII (1640) line (Dawson et al. 2004, 2007; Nagao et al. 2008). In such conditions, the Ly α line becomes a direct measure of the SFR (Kennicutt 1983), which is proportional to the accretion of fresh gas onto the galaxy. The constant of proportionality (the star formation efficiency) between accretion rates and Ly α luminosity is the only free parameter in our models.

This study is organized as follows: In §2 we give a detailed description of our physical model. We describe the DM simulation parameters, and how we generate DM halo catalogs in §3. In §4 we first construct Ly α luminosity function(LF) using model LAEs at $z \approx 3$ and compare it to the observations to find the best-fit model parameter, and then use this best-fit parameter to construct Ly α LFs at $z > 3$. In §5 we derive the physical properties of LAEs using our best-fit model and then investigate the evolution of Ly α LF. We study the large scale structure of model LAEs, and study the redshift evolution of correlation lengths of LAEs in §6. We summarize and present conclusions in §7.

2. PHYSICAL MODEL FOR LYMAN ALPHA EMITTERS

Our model is motivated by the idea that Ly α emission in LAEs is associated with star-formation (Partridge & Peebles 1967) from rapid accretion of new material on to the DM halos. This new material provides fresh fuel to the system driving the star formation (Kereš et al. 2009) and consequently increasing the Ly α line flux in galaxies (Kennicutt 1983; Hu et al. 1999).

In our model we populate each DM halo with an LAE, and assign to it Ly α luminosity ($L_{Ly\alpha}$) proportional to the SFR (Kennicutt 1983; Hu et al. 1999) using the following equation;

$$L_{Ly\alpha} = 1 \times 10^{42} \times \frac{SFR}{M_{\odot} \text{yr}^{-1}} \text{ erg s}^{-1}. \quad (1)$$

Here $L_{Ly\alpha}$ is the intrinsic luminosity of an LAE. The observed Ly α flux will also depend on the escape fraction of the Ly α photons ($f_{esc}^{Ly\alpha}$). Moreover, equation (1) implicitly assumes an escape fraction near zero for the ionizing continuum photons, whose absorption is required to produce the Ly α emission line.

While the escape fraction of ionizing Lyman continuum photons ($\lambda < 912 \text{ \AA}$) is not very precisely known, several studies have shown that an escape fraction of only a few percent is sufficient to meet the observational constraints on the reionization epoch (e.g. Wood & Loeb 2000; Hansen & Oh 2006; Razoumov & Sommer-Larsen 2006; Gnedin et al. 2008). In addition, observations are also generally consistent with small escape fractions of Lyman continuum photons both locally (Leitherer et al. 1995) and at high redshifts (e.g. Steidel et al. 2001; Hansen & Oh 2006; Shapley et al. 2006; Iwata et al. 2009).

The escape fraction of Ly α photons ($f_{esc}^{Ly\alpha}$) is observed to be large with $f_{esc}^{Ly\alpha} \approx 1$ (Gawiser et al. 2006; Kobayashi et al. 2007) likely causing the observed large Ly α equivalent widths (EWs) (Malhotra & Rhoads 2002; Hansen & Oh 2006; Finkelstein et al. 2007). However, the semi-analytic model of Le Delliou et al. (2006) predicts a much smaller value of $f_{esc}^{Ly\alpha} = 2\%$. For simplicity, in our model we approximate $f_{esc}^{Ly\alpha}$ and Lyman continuum photons as unity and zero, respectively. Thus all the Ly α photons produced in LAEs escape to be observed while none of the ionizing photons escape from the galaxy. Small deviations from these assumptions will not affect our results significantly.

As stated earlier, in our model we assume that the rapid accretion of new material on to the DM halos causes star formation in LAEs. We estimate the SFR (mass in accreted gas, ΔM_{gas} converted to stars in unit time) in LAEs by converting baryonic mass accreted (ΔM_b) by DM halos, adopting a constant ratio of baryons to the dark matter, over a short time scale, $t_{Ly\alpha}$. This time scale ($\approx 30 \text{ Myrs}$) is broadly similar to the stellar population ages of most Ly α galaxies (e.g. Pirzkal et al. 2007; Finkelstein et al. 2007, 2008), the lifetimes of OB associations, and the dynamical time expected for Ly α galaxies based on their measured sizes (Pirzkal et al. 2006, 2007). A similar time scale ($\approx 70 \text{ Myrs}$) was used by Shimizu et al. (2007) to match the morphology of large scale structure of LAEs by varying the amplitude of density fluctuations in galaxy formation models.

Thus,

$$SFR = f_{\star} \times \left(\frac{\Delta M_{gas}}{t_{Ly\alpha}} \right) = f_{\star} \times \left(\frac{\Delta M_b}{t_{Ly\alpha}} \right) = f_{\star} \times \dot{M}_b. \quad (2)$$

where f_{\star} is the star formation efficiency. In the above equation we have assumed that ΔM_{gas} is same as the baryonic mass accreted (ΔM_b) by the DM halos, and since our simulation contained only DM particles, we use the universal ratio of baryonic and DM densities i.e. $\Delta M_b = (\Omega_b/\Omega_{DM}) \times \Delta M_{DM}$, where Ω_b and Ω_{DM} are the baryonic and DM density parameters and ΔM_{DM} is the dark matter mass accreted by the DM halos.

Finally, the total mass in *young* stars in an LAE, is

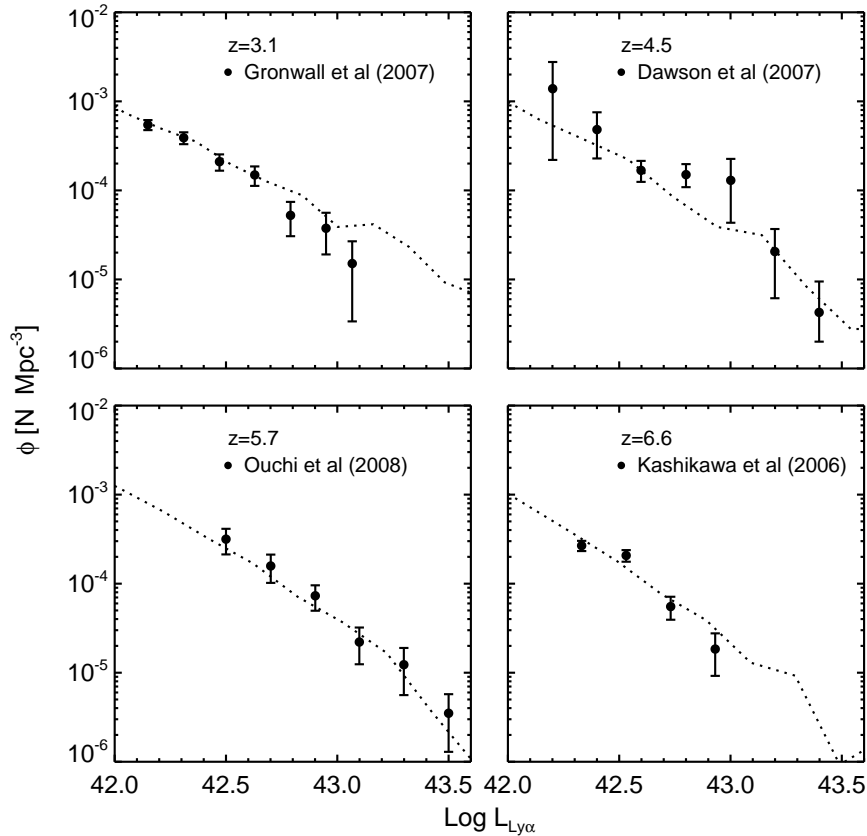


FIG. 1.— Evolution of Ly α LFs at redshifts $z \approx 3 - 7$. The dotted lines show results from our model and the symbols with error bars are the observational data. (a) The best-fit model Ly α LF at $z = 3.1$ yields a star formation efficiency of 2.5%. We use this star formation efficiency to construct model Ly α LFs at $z=4.5, 5.7,$ and 6.6 (b-d). The references for the data: $z = 3.1$ (Gronwall et al. 2007), $z = 4.5$ (Dawson et al. 2007), $z = 5.7$ (Ouchi et al. 2008), and $z = 6.6$ (Kashikawa et al. 2006).

estimated using

$$M_{\star} \approx SFR \times t_{Ly\alpha} = f_{\star} \times \dot{M}_b \times t_{Ly\alpha} = f_{\star} \times \frac{\Omega_b}{\Omega_{DM}} \times \Delta M_{DM}. \quad (3)$$

This corresponds to the mass of stars younger than 30 Myrs which contribute to the Ly α and UV continuum emission, which is more easily measured than the total stellar mass. The only unknown variable in all of the above equations is f_{\star} , the only free parameter in our model.

3. SIMULATION & HALO CATALOGS

We generate the dark matter (DM) halo catalogs using an N-body DM cosmological simulation code GADGET2 (Springel 2005). We generated the initial conditions for the simulation using 2nd-order Lagrangian Perturbation Theory (Crocce et al. 2006; Thacker & Couchman 2006). In this simulation we use 1024^3 DM particles in a comoving volume of $(102 \text{ Mpc})^3$, a volume greater than a typical LAE survey. Each DM particle has a mass $\approx 2.7 \times 10^7 M_{\odot} h^{-1}$. Using Friends-of-Friends (FOF) halo finder, we identify DM halos that contain 100 or more DM particles. This corresponds to a minimum halo mass $\approx 2.7 \times 10^9 M_{\odot} h^{-1}$. We then generate catalogs, for redshifts from $z = 10$ to $z = 3$, which contain positions of

halos, their DM mass, and unique IDs of each individual particle that belongs to a given halo. These unique particle IDs are later used to track halos between two epochs. Throughout this work we assumed a flat Λ CDM cosmology with parameters $\Omega_m=0.233$, $\Omega_{\Lambda}=0.721$, $\Omega_b=0.0462$, $h=0.71$, $\sigma_8=0.817$ where Ω_m , Ω_{Λ} , Ω_b , h , and σ_8 correspond, respectively, to the matter density, dark energy density, and baryonic density in units of the critical density, the Hubble parameter in units of $100 \text{ km s}^{-1} \text{ Mpc}^{-1}$, and the RMS density fluctuations on the $8 \text{ Mpc } h^{-1}$ scale, in agreement with WMAP-5 year results (Hinshaw et al. 2009).

4. LYMAN ALPHA LUMINOSITY FUNCTION

We now construct the Ly α luminosity function (Ly α LF), the number of LAEs per unit volume in a given luminosity bin. First, we calculate the total dark matter mass accreted (ΔM_{DM}) by each DM halo at $z = 3.1$ during an interval ≈ 30 Myrs (equals to $t_{Ly\alpha}$ in equation 2). To calculate ΔM_{DM} we track each halo, using unique ID associated with particles in a given halo, between two epochs separated in time $t_{Ly\alpha}$. In general, we expect every halo to accrete more mass with time. However, due to group finding noise, we find that some halos lose mass with time (negative mass accretion). In other words, the mass accretion by some halos is not real but results from

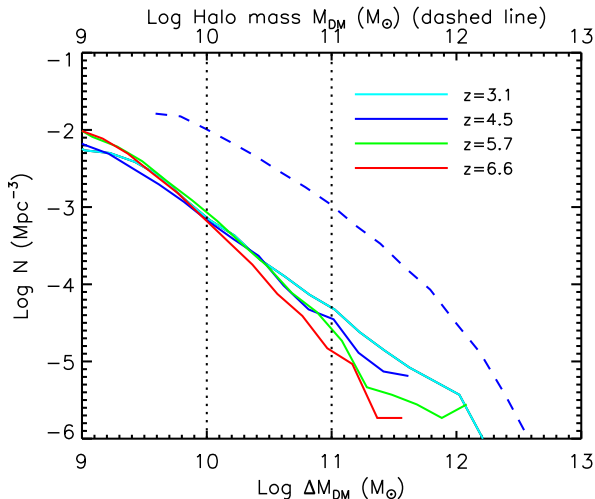


FIG. 2.— Accreted mass function and halo mass functions. Solid lines show accreted mass functions at $z = 3.1$ (violet), $z = 4.5$ (blue), $z = 5.7$ (green) and $z = 6.6$ (red). The dashed blue line shows the dark matter halo mass functions at $z = 4.5$ to compare with the corresponding accreted mass function. The vertical dotted lines enclose the region of observed Ly α luminosities in LAEs.

the simulation noise. The main reason for this noise is the way halos are identified in any DM simulation. In the following paragraph, we discuss how we take into account this noise resulting from the halo finding technique.

In our DM simulation, we use a FOF halo finder that identifies DM halos. In FOF, all the particles within a certain linking length from each other are linked to a halo, independent of whether a given particle is gravitationally bound to a halo. Thus, associating a particle to a halo based on the linking length give rise to some uncertainty in halo mass (in this case ΔM_{DM}). To determine how many halos have real accretion (rather than spurious apparent accretion due to uncertainty in particle association to a halo by the halo finder), we first construct a histogram of ΔM_{DM} including the halos with negative ΔM_{DM} . We then subtract the halo counts in negative ΔM_{DM} bins from the corresponding counts in the positive ΔM_{DM} bins. This procedure compensates for halos that show accretion just due to random nature of FOF halo finder. The residual halos with positive accretion rates are then considered for constructing Ly α LFs.

Next, we convert the accreted mass bins to the Ly α luminosity bins using equation 1 to yield Ly α LF. We then compare this luminosity function with the observations at $z = 3.1$ (Gronwall et al. 2007), and get the best-fit model by varying the star formation efficiency (f_*) to yield the least reduced chi-square (chi-square per degree of freedom) given by

$$\chi_r^2 = \frac{1}{N-1} \sum \frac{(N_{model} - N_{obs})^2}{\sigma_{model}^2 + \sigma_{obs}^2} \quad (4)$$

where N , N_{model} & N_{obs} are the number of observed data points, LAE counts from model, and the observed LAE counts in each bin, respectively, and the Poisson errors are given by $\sigma_{model} = \sqrt{N_{model}}$ and $\sigma_{obs} = \sqrt{N_{obs}}$. Figure 1(top left) shows the best-fit model Ly α LF (dotted line) at $z = 3.1$. The symbols are the observations from

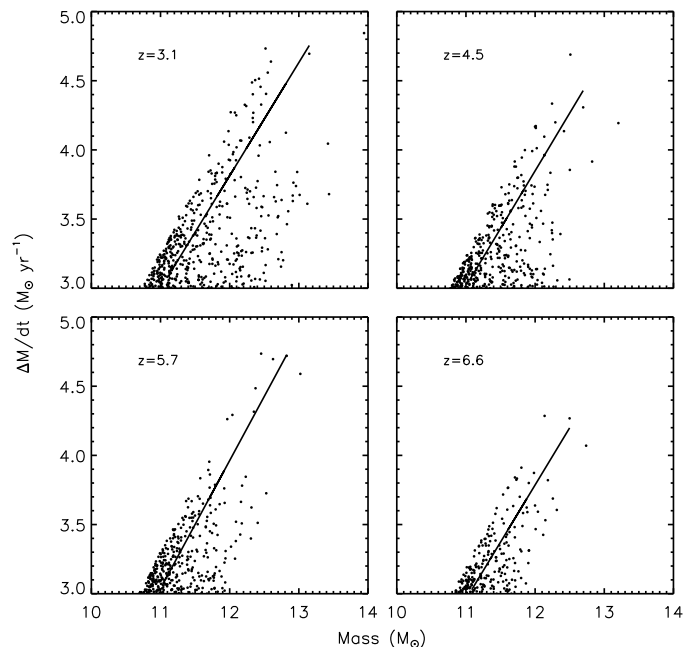


FIG. 3.— The DM accretion rate of halos as a function of halo mass at $z \approx 3 - 7$. The solid line is the least-square fit to the median mass in each $\Delta M/dt$ bin. The slope of the lines is nearly constant $\approx 0.8 - 0.9$ over all redshifts.

Gronwall et al. (2007) shown with 1-sigma error bars.

Lastly, we use the best-fit model parameter *i.e.* the star formation efficiency at $z = 3.1$ to construct the model Ly α LFs at $z > 3$, and then compare these LFs with the observations at $z = 4.5$, 5.7 , and 6.6 . Fig. 1 shows the differential Ly α LFs from our model (dotted lines) and observations (filled circles) at redshifts $z = 3.1$ (Gronwall et al. 2007), $z = 4.5$ (Dawson et al. 2007), $z = 5.7$ (Ouchi et al. 2008), and $z = 6.6$ (Kashikawa et al. 2006). We have rebinned the observational data for $z = 3.1$ and $z = 6.6$ data so as to make the bin size uniform at all redshifts. Wiggles seen, especially in $z = 4.5$ model Ly α LF (Fig. 1 top right) are probably due to simulation noise. The best-fit model for $z = 3.1$ Ly α LF yields a star formation efficiency of 2.5%. Corresponding to this star formation efficiency, the χ_r^2 values between our model and the observed Ly α LFs are 0.5, 0.8, 1.2 & 1.5 for Ly α LFs at $z = 3.1, 4.5, 5.7,$ and 6.6 , respectively.

5. RESULTS

Our model Ly α LFs with single star formation efficiency (SFE), agree remarkably well with the observations. To predict the Ly α LFs of LAEs, Nagamine et al. (2008) investigated two models, the duty cycle & escape fraction scenario, and found that the duty cycle model reproduces observations better than the escape fraction model. In our model, the duty cycle is naturally produced since only halos with high accretion rates will be observed as LAEs. Fig. 2 shows the halo mass function at $z = 4.5$ (blue dashed line) and the accreted mass function (blue solid line). Thus, the use of accreted mass rather than the total halo mass eliminates the need to introduce an additional duty cycle parameter in our model.

A constant SFE over a wide redshift range implies that the physical properties including Ly α luminosity, SFRs, and stellar masses of LAEs do not evolve significantly from $z \approx 3 - 7$ since these properties depend on SFE. Jimenez et al. (2005) also found a similar result of constant SFE (converting accreted baryons to stars) over a wide range (≈ 2 orders of magnitude) of stellar masses, and over a relatively large redshift range, using a large SDSS sample combined with stellar population models. Fig. 3 shows the DM accretion rate as a function of halo mass. The solid line is the least-square fit to the median mass in a $\Delta M/dt$ bin. A nearly constant (0.8-0.9) slope of this line at all redshifts implies that the SFR does not evolve in this redshift range, while deviation of the slopes from unity suggests that the mass accretion rate is a non-linear function of halo mass.

5.1. Physical properties of LAEs

We use the best-fit model parameter (SFE) at $z = 3.1$ to derive other physical properties of LAEs and compare our results with the observations. Our best-fit model yields an SFE of 2.5%, consistent with the global star formation efficiency. Fukugita et al. (1998) predict a SFE $< 5\%$, while Baldry et al. (2008) found this value in the range 4 – 8% for blue light in galaxies.

The SFE of 2.5% yields SFRs $\approx 1 - 10 M_{\odot} \text{ yr}^{-1}$ corresponding to the observed Ly α luminosity range $L_{\text{Ly}\alpha} \approx 1 \times 10^{42} - 1 \times 10^{43} \text{ erg s}^{-1}$. This SFR is comparable to the inferred SFR $\approx 8 M_{\odot} \text{ yr}^{-1}$ in LAEs at $z \approx 5$ (Pirzkal et al. 2007). A similar average value of SFR $\approx 6 M_{\odot} \text{ yr}^{-1}$ was inferred for $z = 3.1$ LAEs (Gawiser et al. 2006). A slightly higher value of SFR $\approx 5.7 - 28.3 M_{\odot} \text{ yr}^{-1}$ with median SFR $\approx 9.6 M_{\odot} \text{ yr}^{-1}$ was inferred for $z = 5.7$ LAEs (Murayama et al. 2007). For $z = 6.6$ LAEs, Taniguchi et al. (2005) found an average SFR $\approx 5.7 \pm 2.3 M_{\odot} \text{ yr}^{-1}$. These averages however depend on the depth of the surveys; deeper surveys probe less luminous galaxies and hence lower SFRs.

The total stellar mass in young stars (estimated using equation 3) of LAEs corresponding to the observed Ly α luminosity range is $M_{\star} \approx 3 \times 10^7 - 3 \times 10^8 M_{\odot}$, in good agreement with the observed stellar masses of $10^7 M_{\odot} - 10^9 M_{\odot}$ for a LAE sample at $z = 4.5$ (Finkelstein et al. 2007; Gawiser et al. 2007; Pirzkal et al. 2007; Pentericci et al. 2009). Thus, our model reproduces the primary physical properties of LAEs at $z \approx 3 - 7$. In addition, our assumption of large escape fraction of Ly α photons will yield high observed equivalent widths of Ly α line in LAEs.

5.2. Evolution of Ly α luminosity function

The Ly α LFs have been used to probe the epoch of reionization and constrain the evolution of intergalactic medium (IGM) (e.g. Haiman & Spaans 1999; Malhotra & Rhoads 2004; Haiman & Cen 2005; Stern et al. 2005; Kashikawa et al. 2006; Dijkstra et al. 2007; McQuinn et al. 2007; Mesinger & Furlanetto 2008; Ota et al. 2008). Any significant evolution of the Ly α LF, after correcting for the intrinsic change in the number density of LAEs, between two redshifts will imply that the IGM evolved at these redshifts.

Currently the evolution of Ly α LF at $z > 5$ is not well understood. Previous studies find no significant

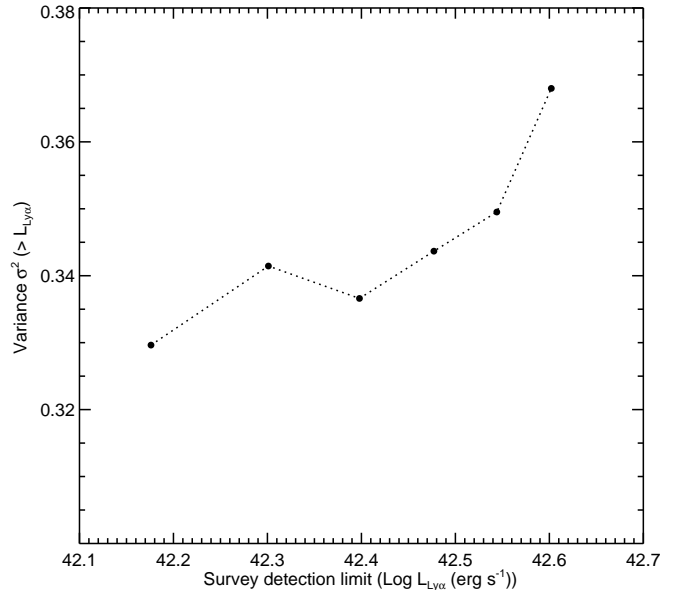


FIG. 4.— Field-to-field variance of number of LAEs at $z = 6.6$, measured in eight subvolumes ($102 \times 51 \times 25 \text{ Mpc}^3$), plotted as a function of survey detection limit. The variance $\sigma^2 > 30\%$ for a typical narrow-band LAE survey with Ly α detection limit $> 2 \times 10^{42} \text{ erg s}^{-1}$.

evolution in Ly α LFs at redshifts between $z = 5.7$ and $z = 6.5$ (Malhotra & Rhoads 2004). However recent observations (Kashikawa et al. 2006; Ota et al. 2008) find a modest decline in the bright end of the Ly α LF from $z = 5.7$ to $z = 6.6$, suggesting IGM evolution at these redshifts. Dijkstra et al. (2007) showed that the weak IGM evolution between $z = 5.7$ & $z = 6.6$ can be attributed to the evolution of DM halo mass function. In addition, the cosmic variance in a volume limited LAE survey also affects the Ly α LFs. For example, Shioya et al. (2009) find that the number density of LAEs, at $z \approx 5$ vary by a factor ≈ 2 in a survey area of $0.5^\circ \times 0.5^\circ$. We now investigate the evolution of Ly α LFs, and the effect of cosmic variance on number density of LAEs in a volume and flux limited LAE survey.

From Fig. 2 we see that there is some evolution of number density of DM halos that can host LAEs. However, this weak evolution is due to the intrinsic change in the number density since we haven't included any IGM correction in our model. Thus our model can explain the observed evolution of Ly α LF (Kashikawa et al. 2006) without invoking the cosmic variance. However, it would be interesting to estimate the effect of cosmic variance on the Ly α LF.

In order to understand the effect of cosmic variance on the observed number density of LAEs in a volume and flux limited LAE survey, we estimate the field-to-field variance by dividing the total simulation volume into eight non-overlapping rectangular boxes, each with a comoving volume ($102 \times 51 \times 25 \text{ Mpc}^3$) comparable to typical narrow-band LAE surveys. The variance is calculated using $\sigma^2 = \langle (N - \mu)^2 \rangle / \mu$, where N is the number of LAEs in each sub-volume and μ is the average number of LAEs. Fig. 4 shows field-to-field variance, for a volume limited LAE survey with different Ly α flux limit. For a narrow-band LAE survey with Ly α detec-

tion limit of $L_{Ly\alpha} > 2 \times 10^{42}$ erg s $^{-1}$ and a survey volume $< 2 \times 10^5$ Mpc 3 , the field-to-field variation is significant with $\sigma^2 \gtrsim 30\%$. This result confirms the necessity of using a large volume to minimize cosmic variance in LAE surveys. It also strengthens our conclusion that some apparent evolution of Ly α LF can be attributed to the cosmic variance.

6. CLUSTERING OF LAES

LAEs are found to trace rarer, higher density regions (Iliev et al. 2008; Orsi et al. 2008). However, Shimizu et al. (2007) suggested that the LAEs at $z \approx 3$ do not necessarily reside in high density peaks. In this section, we investigate whether our model LAEs reside in high density regions, and estimate their spatial correlation lengths. Fig. 5 shows the spatial distribution of LAEs at two different redshifts, $z = 5.7$ and $z = 4.5$, in a simulation slice of $30 \times 30 \times 17 h^{-3}$ Mpc 3 . The depth of this slice is comparable to the depth of a typical LAE survey. Comparing the locations of LAEs at two redshifts it is clear that different halos host LAEs at different redshifts, thus exhibiting a duty cycle (Stark et al. 2007; Nagamine et al. 2008). Our model LAEs are generally located around overdense regions consistent with the observations and as expected in biased galaxy formation models.

6.1. Two-point spatial correlation function

The two-point spatial correlation function $\xi(r)$ (Peebles 1980) is frequently used to study the clustering properties of galaxies (e.g. Zehavi et al. 2005; Gawiser et al. 2007; Kovač et al. 2007). We use the Landy-Szalay estimator, proposed by Landy & Szalay (1993), to calculate the two-point spatial correlation function given by

$$\xi(r) = \frac{DD(r) - 2DR(r) + RR(r)}{RR(r)}, \quad (5)$$

where $DD(r)$, $RR(r)$, and $DR(r)$ are the number of galaxy-galaxy, random-random and galaxy-random pairs, respectively with separation distance of $(r, r + \delta r)$. To compare our model $\xi(r)$ with the observations and quantify its evolution with redshift we only include LAEs brighter than the detection limit of LAE surveys at a given redshift, and use our full simulation volume $\approx 1 \times 10^6$ Mpc 3 for better statistical significance.

To calculate $\xi(r)$ at each redshift, we generated a random sample of points with uniform coordinates drawn from a uniform probability distribution, and a number of random points exactly equal to the number of LAEs. We count the number of pairs, $DD(r)$, $RR(r)$, and $DR(r)$ separated by a distance r by binning the points at different r with binwidth of $\delta r = 0.2 h^{-1}$ Mpc. To minimize the random errors, we perform 50 realizations with different sets of random points and calculate an average $\xi(r)$ at each r . Using $r < 20 h^{-1}$ Mpc and assuming negligible error, we obtain the spatial correlation length r_0 by fitting a least-square power law to the correlation function.

The correlation lengths obtained from our model LAEs show a modest evolution, with $r_0 = (3.2 \pm 0.3, 5.0 \pm 0.3, 4.2 \pm 0.6, 6.0 \pm 1) h^{-1}$ at $z = (3.1, 4.5, 5.7, 6.6)$, respectively. Fig. 6 (*left*) shows a comparison between our

model predictions (filled circles) and observed r_0 (shown with different symbols given in the labels) at different redshifts. The model predicted r_0 values are slightly shifted along x-axis to avoid overlap with the observations. The predicted correlation lengths are consistent with the observations at $z = 3.1$ with observed $r_0 = 2.6 \pm 1 h^{-1}$ (Gawiser et al. 2007), and at $z = 4.5$ with observed $r_0 = 4.6 \pm 0.6 h^{-1}$ (Kovač et al. 2007) estimated using contamination-corrected (the maximum value permitted) LAE sample. However, Ouchi et al. (2003) found a higher $r_0 = 6.2 \pm 0.5 h^{-1}$ Mpc for contamination-corrected LAE sample $z = 4.86$. It would be interesting to estimate the variance of r_0 in a volume and flux limited LAE survey, and see if we can account for the large difference seen in the observed r_0 between $z = 4.5$ & $z = 4.86$ LAE surveys.

To estimate the variance of r_0 ($\sigma_{r_0}^2$) in a volume and flux limited LAE survey, we divide the total simulation volume at $z = 3.1$ into five non-overlapping sub-volumes, each with a comoving volume of $(102 \times 102 \times 20.4)$ Mpc 3 , approximately equal to a typical survey volume and only including LAEs with $L_{Ly\alpha} > 1 \times 10^{42}$ erg s $^{-1}$. We calculate $\xi(r)$ and r_0 , as described above (second paragraph) in each sub-volume and estimate $\sigma_{r_0}^2$ at $z = 3.1$. We find $\sigma_{r_0}^2 = 0.5 h^{-1}$ Mpc with an average $r_0 = 3.2 h^{-1}$ Mpc, average of r_0 in five sub-volumes. While this variance in r_0 cannot account for the large difference in r_0 observed between the two surveys at $z = 4.5$ & 4.86, it is clear that one needs to take into account such variance in correlation lengths obtained from volume and flux limited surveys.

We now investigate if the redshift evolution of r_0 seen in Fig. 6 (*left* panel) is significant since this redshift evolution can result from the surveys at lower redshifts extending to lower luminosities and hence probing lower halo masses. In order to understand this effect, we consider full simulation volume and only include LAEs with a constant $L_{Ly\alpha} > 1 \times 10^{42}$ erg s $^{-1}$ at all redshifts. Choosing a constant lower luminosity at all redshifts implies that we are probing approximately same halo masses at all redshifts. We calculate r_0 in the same way as described above (second paragraph) except that we impose a constant luminosity cutoff at all redshifts. Fig. 6 (*right* panel) shows r_0 with a constant lower luminosity at all redshifts. While the predicted correlation length show some evolution with redshift, even after applying a constant lower luminosity cutoff at all redshifts, most of this evolution seen in Fig. 6 (*left* panel) can be attributed to the luminosity limit of different surveys probing different halo masses. In order to test our model predictions, we suggest that more LAE observations are necessary for probing a wider range of halo masses especially at $z > 5$.

7. SUMMARY AND CONCLUSIONS

We have used a physical model with a single variable parameter to populate dark matter (DM) halos with LAEs in a cosmological simulation and compared our model predictions with the observations at redshifts $z \approx 3 - 7$. In our model we assumed that the star formation rate (SFR), and hence the Ly α line luminosity is proportional to the mass accreted by halos. In other words, the star formation in LAEs mainly results from the cold accretion of new material. Despite the lack of

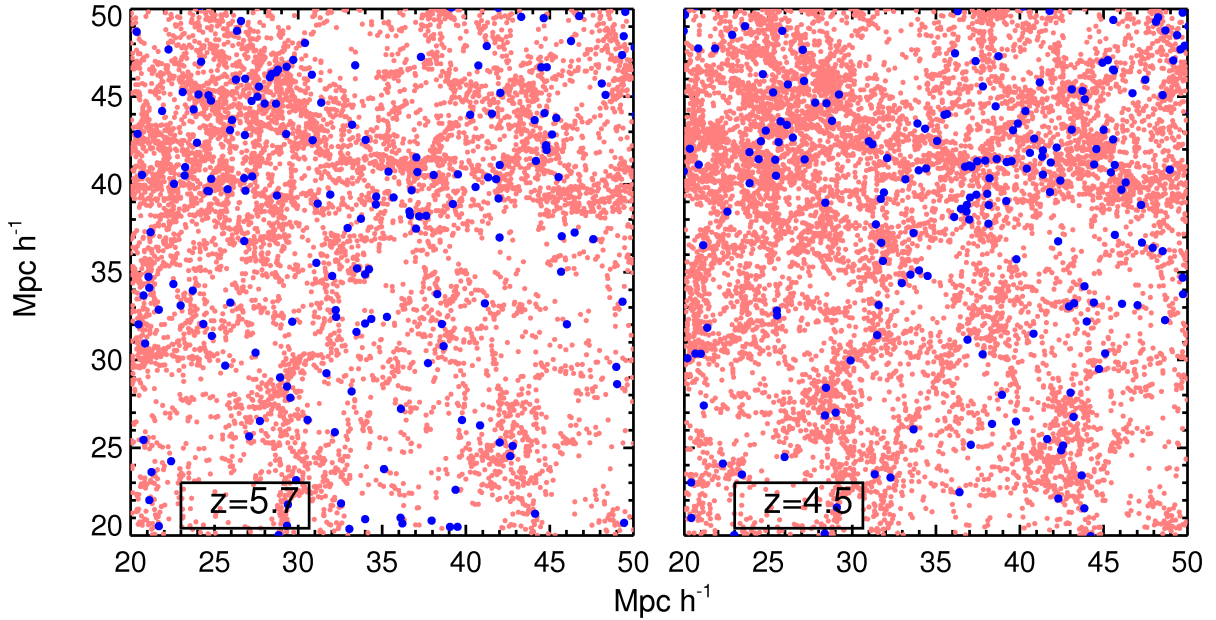


FIG. 5.— The spatial distribution of our model LAEs in a slice from DM simulation at two redshifts $z = 5.7$ (left) and $z = 4.5$ (right) in a volume $30 \times 30 \times 17 h^{-3} \text{ Mpc}^3$. The small (red) and big (blue) filled circles represent the positions of DM halos and model LAEs, respectively. Only LAEs with $L_{Ly\alpha} > 2 \times 10^{42} \text{ erg s}^{-1}$ are plotted. In general, the LAEs are located in high density regions. Also note that different halos host LAEs at the two redshifts, depending on whether they are accreting or not. This gives rise to a duty cycle quite naturally.

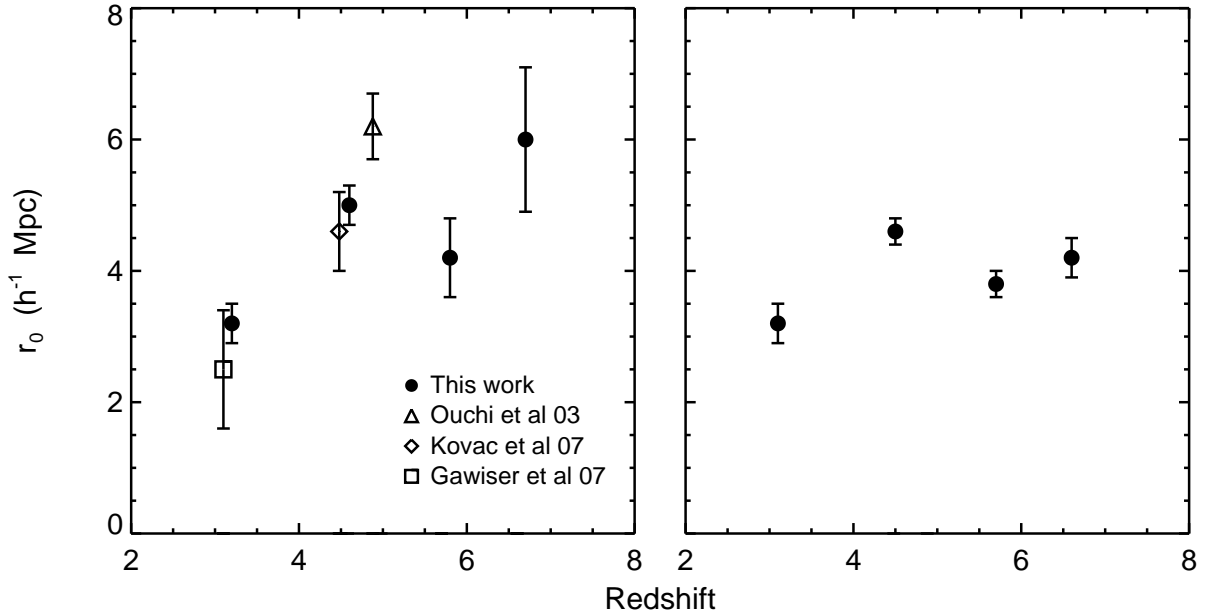


FIG. 6.— Correlation lengths of LAEs at different redshifts. *Left*. Comparison of correlation lengths of our model and observed LAEs at different redshifts. Here we include LAEs with $Ly\alpha$ luminosity greater than the survey limit at each redshift. The filled circles are our model results, other symbols are from different observations as shown in the labels. The observed r_0 values shown here for $z=4.5$ & 4.86 are for the contamination corrected (the maximum value permitted) LAE sample. Our model results are slightly shifted to avoid overlap with other observational points. *Right*. The correlation lengths of our model LAEs with a constant $Ly\alpha$ luminosity cutoff ($L_{Ly\alpha} > 1 \times 10^{42} \text{ erg s}^{-1}$) at all redshifts.

observational evidence relating accretion rate to the $Ly\alpha$

luminosity of LAEs, it is promising that our model gives

good fit to the observations over a wide range of redshifts and is able to reproduce several other physical properties of LAEs. In addition, relating the accreted mass (rather than the total halo mass) to the Ly α luminosity, gives rise to a duty cycle of LAEs (Nagamine et al. 2008) quite naturally.

To compare our model predictions with the observations, we first constructed the Ly α luminosity function (LF) at $z = 3.1$ and obtained the best-fit model by varying the star formation efficiency (SFE) and comparing the model Ly α LF with the observations at this redshift. We then used this best-fit model to predict the Ly α LFs and physical properties of LAEs at $z = 4.5, 5.7$ and $z = 6.6$.

Using a constant SFE, our model predicted Ly α LFs agree remarkably well with the LAE observations over a wide redshift range. Since other physical properties including SFR and stellar masses of LAEs depend on SFE, it implies that these properties do not evolve significantly over these redshift range. Our best-fit model yields a SFE=2.5% which gives SFR $\approx 1 - 10 M_{\odot}\text{yr}^{-1}$ in good agreement with the observations. We find that the model LAEs in the currently observable luminosity range ($2 \times 10^{42} \lesssim L_{\text{Ly}\alpha} \lesssim 2 \times 10^{43} \text{erg s}^{-1}$) have stellar masses $\approx 3 \times 10^7$ to $3 \times 10^8 M_{\odot}$ of young (< 30 Myr) stars. These stellar masses of LAEs are similar to those inferred from observations (Finkelstein et al. 2007; Pirzkal et al. 2007). We also investigated the evolution of Ly α LFs from $z \approx 3 - 7$ and find that there is no significant evolution of Ly α LF due to the IGM if we include the intrinsic change in the number density of LAEs over this redshift range. This conclusion is strengthened if we include the

effect of cosmic variance on the observed number density of LAEs. We show that the field-to-field variance can be large $\approx 30\%$ for a flux and volume limited surveys comparable to current observations.

We studied the clustering properties of LAEs and found that the LAEs are mostly located in the high density peaks. Our model predicted correlation lengths $r_0 = (3.2 \pm 0.3, 5.0 \pm 0.3)h^{-1}$ Mpc which are in good agreement with the observations. We also estimate the variance in r_0 ($\sigma_{r_0}^2$) in a volume and flux limited LAE survey and find that $\sigma_{r_0}^2 = 0.5 h^{-1}$ Mpc at $z = 3.1$. Our model predicts a modest evolution of r_0 with redshifts and we have shown that most of this redshift evolution can be attributed to the luminosity limit of LAE surveys. Currently, there are no measurements of r_0 at $z > 5$ due to insufficient sample size of LAEs at higher redshifts. Therefore, more data is needed to test our predictions at higher redshifts in order to understand the evolution of r_0 with redshifts.

This work was supported in part by the School of Earth & Space Exploration, Arizona State University, the NSF grant AST-0808165, the Swiss National Science Foundation grant 200021-116696/1 and Swedish Research Council grant 60336701. RJT is supported by a Discovery Grant from NSERC, the Canada Research Chairs program & the Canada Foundation for Innovation. All simulations were conducted on the *Saguaro* cluster operated by the Fulton School of Engineering at Arizona State University.

REFERENCES

- Ajiki, M., et al. 2003, AJ, 126, 2091
 Baldry, I. K., Glazebrook, K., & Driver, S. P. 2008, MNRAS, 388, 945
 Barton, E. J., Davé, R., Smith, J.-D. T., Papovich, C., Hernquist, L., & Springel, V. 2004, ApJ, 604, L1
 Cowie, L. L., & Hu, E. M. 1998, AJ, 115, 1319
 Crocce, M., Pueblas, S., & Scoccimarro, R. 2006, MNRAS, 373, 369
 Davé, R., Finlator, K., & Oppenheimer, B. D. 2006, MNRAS, 370, 273
 Dawson, S., et al. 2004, ApJ, 617, 707
 Dawson, S., Rhoads, J. E., Malhotra, S., Stern, D., Wang, J., Dey, A., Spinrad, H., & Jannuzi, B. T. 2007, ApJ, 671, 1227
 Dekel, A., Sari, R., & Ceverino, D. 2009, arXiv:0901.2458
 Dijkstra, M., Wyithe, J. S. B., Haiman, Z. 2007, MNRAS, 379, 253D
 Fernandez, E. R., & Komatsu, E. 2008, MNRAS, 384, 1363
 Finkelstein, S. L., Rhoads, J. E., Malhotra, S., Pirzkal, N., & Wang, J. 2007, ApJ, 660, 1023
 Finkelstein, S. L., Rhoads, J. E., Malhotra, S., Grogin, N., & Wang, J. 2008, ApJ, 678, 655
 Fukugita, M., Hogan, C. J., & Peebles, P. J. E. 1998, ApJ, 503, 518
 Fynbo, J. U., Möller, P., & Thomsen, B. 2001, A&A, 374, 443
 Gawiser, E., et al. 2006, ApJ, 642, L13
 Gawiser, E., et al. 2007, ApJ, 671, 278
 Gnedin, N. Y., Kravtsov, A. V., & Chen, H.-W. 2008, ApJ, 672, 765
 Gronwall, C., et al. 2007, ApJ, 667, 79
 Hansen, M., & Oh, S. P. 2006, MNRAS, 367, 979
 Haiman, Z., & Cen, R. 2005, ApJ, 623, 627
 Haiman, Z., & Spaans, M. 1999, ApJ, 518, 138
 Hinshaw, G., et al. 2009, ApJS, 180, 225
 Hu, E. M., McMahon, R. G., & Cowie, L. L. 1999, ApJ, 522, L9
 Iliev, I. T., Shapiro, P. R., McDonald, P., Mellema, G., & Pen, U.-L. 2008, MNRAS, 391, 63
 Iwata, I., et al. 2009, ApJ, 692, 1287
 Jimenez, R., Panter, B., Heavens, A. F., & Verde, L. 2005, MNRAS, 356, 495
 Kashikawa, N., et al. 2006, ApJ, 648, 7
 Kennicutt, R. C., Jr. 1983, ApJ, 272, 54
 Kereš, D., Katz, N., Fardal, M., Davé, R., & Weinberg, D. H. 2009, MNRAS, 395, 160
 Kobayashi, M. A. R., Totani, T., & Nagashima, M. 2007, ApJ, 670, 919
 Kovač, K., Somerville, R. S., Rhoads, J. E., Malhotra, S., & Wang, J. 2007, ApJ, 668, 15
 Landy, S. D., & Szalay, A. S. 1993, ApJ, 412, 64
 Le Delliou, M., Lacey, C. G., Baugh, C. M., & Morris, S. L. 2006, MNRAS, 365, 712
 Leitherer, C., Ferguson, H. C., Heckman, T. M., & Lowenthal, J. D. 1995, ApJ, 454, L19
 Malhotra, S., & Rhoads, J. E. 2002, ApJ, 565, L71
 Malhotra, S., Wang, J. X., Rhoads, J. E., Heckman, T. M., & Norman, C. A. 2003, ApJ, 585, L25
 Malhotra, S., & Rhoads, J. E. 2004, ApJ, 617, L5
 Mao, J., Lapi, A., Granato, G. L., de Zotti, G., & Danese, L. 2007, ApJ, 667, 655
 Matsuda, Y., et al. 2005, ApJ, 634, L125
 McQuinn, M., Hernquist, L., Zaldarriaga, M., & Dutta, S. 2007, MNRAS, 381, 75
 Mesinger, A., & Furlanetto, S. R. 2008, MNRAS, 386, 1990
 Murayama, T., et al. 2007, ApJS, 172, 523
 Nagamine, K., Ouchi, M., Springel, V., & Hernquist, L. 2008, arXiv:0802.0228
 Nagao, T., et al. 2008, ApJ, 680, 100
 Nilsson, K. K., et al. 2007, A&A, 471, 71
 Orsi, A., Lacey, C. G., Baugh, C. M., & Infante, L. 2008, MNRAS, 391, 1589

- Ota, K., et al. 2008, ApJ, 677, 12
Ouchi, M., et al. 2008, ApJS, 176, 301
Ouchi, M., et al. 2003, ApJ, 582, 60
Partridge, R. B., & Peebles, P. J. E. 1967, ApJ, 147, 868
Peebles, P. J. E. 1980, Research supported by the National Science Foundation. Princeton, N.J., Princeton University Press, 1980. 435 p
Pentericci, L., Grazian, A., Fontana, A., Castellano, M., Giallongo, E., Salimbeni, S., & Santini, P. 2009, A&A, 494, 553
Pirzkal, N., et al. 2006, ApJ, 636, 582
Pirzkal, N., Malhotra, S., Rhoads, J. E., & Xu, C. 2007, ApJ, 667, 49
Razoumov, A. O., & Sommer-Larsen, J. 2006, ApJ, 651, L89
Rhoads, J. E., Malhotra, S., Dey, A., Stern, D., Spinrad, H., & Jannuzi, B. T. 2000, ApJ, 545, L85
Rhoads, J. E., et al. 2004, ApJ, 611, 59
Scannapieco, E., & Thacker, R. J. 2003, ApJ, 590, L69
Shapley, A. E., Steidel, C. C., Pettini, M., Adelberger, K. L., & Erb, D. K. 2006, ApJ, 651, 688
Shimizu, I., Umemura, M., & Yonehara, A. 2007, MNRAS, 380, L49
Shioya, Y., et al. 2009, ApJ, 696, 546
Shimasaku, K., et al. 2006, PASJ, 58, 313
Springel, V. 2005, MNRAS, 364, 1105
Stark, D. P., Loeb, A., & Ellis, R. S. 2007, ApJ, 668, 627
Steidel, C. C., Pettini, M., & Adelberger, K. L. 2001, ApJ, 546, 665
Stern, D., Yost, S. A., Eckart, M. E., Harrison, F. A., Helfand, D. J., Djorgovski, S. G., Malhotra, S., & Rhoads, J. E. 2005, ApJ, 619, 12
Tapken, C., et al. 2006, A&A, 455, 145
Taniguchi, Y., et al. 2005, PASJ, 57, 165
Tasitsiomi, A. 2006, ApJ, 645, 792
Thacker, R. J. & Couchman, H. M. P., 2006, Int. J. High Perf. Comp. & Net., 4, 303
Venemans, B. P., et al. 2005, A&A, 431, 793
Wang, J. X., et al. 2004, ApJ, 608, L21
Wood, K., & Loeb, A. 2000, ApJ, 545, 86
Zehavi, I., et al. 2005, ApJ, 630, 1